Trion-Induced Negative Photoconductivity in Monolayer MoS_{2}

C. H. Lui, A. J. Frenzel, D. V. Pilon, Y.-H. Lee, X. Ling, G. M. Akselrod, J. Kong, and N. Gedik

Phys. Rev. Lett. **113**, 166801 — Published 16 October 2014

DOI: 10.1103/PhysRevLett.113.166801

Trion induced negative photoconductivity in monolayer MoS_2

C. H. Lui[1], A. J. Frenzel[1,2], D. V. Pilon[1], Y.-H. Lee[3,4], X. Ling[3], G. M. Akselrod[1], J. Kong[3], and N. Gedik[1*]

[1]*Department of Physics, Massachusetts Institute of Technology, Cambridge, Massachusetts 02139, USA*

[2]*Department of Physics, Harvard University, Cambridge, Massachusetts 02138, USA*

[3]*Department of Electrical Engineering and Computer Science, Massachusetts Institute of Technology, Cambridge, Massachusetts 02139, USA*

[4]*Department of Materials Science and Engineering, National Tsing Hua University, Hsinchu 30013, Taiwan*

**email: gedik@mit.edu*

Abstract: Optical excitation typically enhances electrical conduction and low-frequency radiation absorption in semiconductors. We have, however, observed a pronounced transient *decrease* of conductivity in doped monolayer molybdenum disulfide (MoS_2), a two-dimensional (2D) semiconductor, using ultrafast optical-pump terahertz-probe spectroscopy. In particular, the conductivity is reduced to only 30% of its equilibrium value at high pump fluence. This anomalous phenomenon arises from the strong many-body interactions in the 2D system, where photoexcited electron-hole pairs join the doping-induced charges to form trions, bound states of two electrons and one hole. The resultant increase of the carrier effective mass substantially diminishes the conductivity.

Atomically thin transition metal dichalcogenides (TMDs, e.g. MoS_2, $MoSe_2$, WS_2, WSe_2) are two-dimensional (2D) semiconductors with rich physical properties, including high mechanical strength and flexibility, strong photoluminescence (PL) [1,2], superior (opto)electronic performance [3,4], and intriguing coupled spin-valley physics [5-8]. These remarkable properties make TMD materials promising for developing next-generation (opto)electronics and spin-valleytronics. One distinctive feature of monolayer TMDs is the strong quantum confinement and reduced dielectric screening in the strict 2D limit. The resultant strong Coulomb interactions cause photoexcited electron-hole pairs to form tightly bound excitons, which govern the optical and electronic properties of the materials [9-22]. In samples with excess charges, the excitons can capture additional charges to form trions (charged excitons). These trions possess exceptionally high dissociation energies (20 - 50 meV), and their concentration and spin/valley configuration can be controlled by electrical gate and optical helicity, respectively [12,23-25]. Although these strong many-body effects have been observed in 2D TMDs, their influence on the materials' intrinsic conductive behavior and implications for device applications have not been explored thus far.

In this letter, we report the first experimental signature of a profound trionic effect on the conductive properties of atomically thin TMD materials. By using time-resolved terahertz (THz) spectroscopy [26,27], we have observed an anomalous transient *decrease* of THz conductivity in doped monolayer MoS_2 after femtosecond laser excitation at T = 4 - 350 K. The negative photoconductivity saturates at high pump fluence, where the conductivity is substantially reduced to ~30% of its equilibrium value. This behavior contrasts with the positive photoconductivity found in multilayer and bulk MoS_2, and in other conventional semiconductors (e.g. Si, Ge and GaAs) [26,27]. Our results reflect the strong many-body interactions in

monolayer MoS_2, where photoexcited carriers form trions with the original free electrons. The resultant increase of effective mass significantly diminishes the carrier mobility and conductivity. This interaction-driven photo-reduction of conductivity represents an intrinsic property of monolayer MoS_2 crystals, in contrast to the negative photoconductivity arising from trapping or spatial transfer of charges in some semiconductor systems with high defect density or heterogeneous structure [28,29].

To reveal the intrinsic conductive properties of monolayer MoS_2, we used time-domain THz spectroscopy. This approach avoids the complication of electrical contacts in transport experiments, and when applied with femtosecond laser excitation, can probe short-lived excited carriers prior to trapping or recombination [26,27]. Our experiment employed a 5-kHz Ti:sapphire amplifier system that generates laser pulses with 1.55 eV photon energy and 90 fs pulse duration. The laser was split into two beams. One beam was frequency-converted through an optical parametric amplifier (OPA) and/or second harmonic generation for pumping the sample. The other beam generated THz pulses by optical rectification in a ZnTe crystal for probing the sample. By using electro-optic sampling detection, we could map out the whole waveform of the THz electric field E(t) in the time domain, and the pump-induced change of the field $\Delta E(t, \tau)$ at a controllable pump-probe delay time τ [30-32].

We investigated large-area monolayer MoS_2 samples grown by chemical vapor deposition (CVD) on sapphire substrates [33,34]. The samples were mounted on a helium-flow cryostat in high vacuum. We first measured their THz absorption in equilibrium conditions at T = 15 K. We recorded the THz electric field transmitted through the MoS_2/substrate area, E(t), and as a reference, through an area without MoS_2 flakes, $E_0(t)$ [Fig. 1(a)]. The maximum value of E(t) was 2.1% smaller than that of $E_0(t)$. This attenuation of the THz transmission [insets of Fig.

1(a)] arises from intraband absorption of excess free electrons in the doped sample. From the measured transmission spectra, we extracted the complex sheet conductivity of monolayer MoS_2 by applying the standard thin-film approximation [30,35,36]. We determined in the spectral range of 0.5 - 2.0 THz an average (real) conductivity $\sigma_1 \approx 2 \pm 0.5\ G_0$, where $G_0 = 2e^2/h$ is the quantum of conductance. We estimated the doping electron density of our samples to be $n \approx 5.5 \pm 2 \times 10^{12}$ cm^{-2} from the trion dissociation energy (~40 meV) [see the PL spectra in the inset of Fig. 5(a)], which increases with the Fermi level according to Ref. [23]. We then obtained an electron mobility $\mu = \sigma_1/ne \approx 180 \pm 70$ $cm^2V^{-1}s^{-1}$ for our samples at T = 15 K.

To investigate the optoelectronic response of monolayer MoS_2, we excited the sample using 3.1-eV laser pulses. Excitation at this photon energy, with fluences used in our experiment, can generate 10^{13}~10^{14} carriers/cm^2 in the MoS_2 monolayer [37], which is expected to greatly enhance the THz absorption (e.g. see Fig. 11 in Ref. [27]). Surprisingly, our result of pump-induced change of transmission (proportional to ΔE) indicates a transient *decrease* of THz absorption in the monolayer MoS_2 sample [Fig. 1(b)] [30]. To further explore this unusual behavior, we have measured the temporal (τ) evolution of the fractional change of the THz field, i.e. the ratio between the maximum values of waveforms $\Delta E(t,\tau)$ and $E(t)$ [Fig. 1(c)]. The THz dynamics exhibit a short component with lifetime $\tau_1 \approx 1$ ps, followed by a long component with lifetime $\tau_2 \approx 42$ ps. From the measured transmission spectra, we extracted the change of complex sheet conductivity $\Delta\sigma(\omega,\tau)$ of monolayer MoS_2 [30]. Both the real and imaginary parts of $\Delta\sigma(\omega,\tau)$ exhibit negative values for all delay times (τ) and frequencies (ω) in our measurement range [Fig. 1(d)].

The observed negative photoconductivity is a robust and substantial effect in monolayer MoS_2. It persists for all incident pump fluences ($F = 0.4 - 170$ $\mu J/cm^2$) and temperatures (T = 4

– 350 K) in our experiment [see, for example, fluence dependence in Fig. 2(a-b) and data for T = 300 K in Fig. 2(c)]. As the pump fluence increases, the reduction of the THz absorption increases and gradually saturates at ~70% decrease of the total absorption [Fig. 2(b)], indicating that the conductivity of monolayer MoS_2 is reduced to only ~30% of its equilibrium value. The long component exhibits considerable increase of magnitude and relaxation time with the fluence, and becomes the dominant contribution to the overall dynamical response in the saturation regime [Fig. 2(a-b)].

Negative photoconductivity was observed in monolayer MoS_2 samples deposited on sapphire and quartz substrates, with and without HfO_2 or polymer electrolyte top layers. The insensitivity to the dielectric and interfacial environment implies that the phenomenon originates from the intrinsic property of the MoS_2 material. We also examined multilayer CVD MoS_2 films and bulk MoS_2 crystals. We did not observe any photo-reduction of conductivity in these thicker samples, but only the expected photo-enhancement (see Supplemental Material [30]).

We can understand the above observations by considering the substantially enhanced Coulomb interaction and excitonic effects in monolayer MoS_2. The binding energies of excitons in MoS_2 and other TMD monolayers have been estimated to be a few hundred meV [9-22], an order of magnitude larger than the values of their respective multilayer and bulk crystals [11,38]. As excited carriers in MoS_2 are known to relax within 100 fs [39], we expect the photo-generated electrons and holes to form tightly bound excitons in monolayer MoS_2 almost instantaneously. These excitons are charge neutral and have resonance energies much higher than the THz photon energy (~4 meV). They will not interact with the THz radiation and change the THz conductivity. This accounts for the lack of positive THz photoconductivity in monolayer MoS_2 at all pump fluences in our experiment. We note that our THz technique is different from

conventional transport methods, in which a large DC electric field is applied across the samples to break the excitons into free carriers, thus leading to positive photoconductivity [1,4,21,40].

To account for the negative photoconductivity, we further consider the interactions between the excitons and free charges. Previous experiments [12,23-25] have shown that when excess doped electrons are available, the excitons can capture free electrons to form three-body bound states with two electrons and one hole in monolayer MoS_2 and other TMDs. These complex quasiparticles, the so-called trions or charged excitons, possess large dissociation energies (20 – 50 meV) and are stable even at room temperature. Trion formation can adequately account for our experimental observations: after pulsed excitation, the generated electron-hole pairs form trions with the excess free charges within the rise time of the pump-probe signal (~1 ps). The trions behave as free charged particles with increased effective mass [41], resulting in lower carrier mobility (μ) and hence lower conductivity ($\sigma_1 = ne\mu$). In other words, instead of increasing the free-carrier concentration, photoexcitation adds mass to the original free charges and dulls their response to the electric field (Fig. 3).

A straightforward way to confirm the trion scheme is to compare the THz dynamics with the trion decay dynamics. We have carried out time-resolved PL measurements on our monolayer MoS_2 samples at T = 300 K [Fig. 2(d)] [30]. The PL intensity in the emission photon energy range of 1.7 - 2.0 eV [inset of Fig. 5(a)] is proportional to the trion population and decayed with a lifetime of $\tau_2 = 33 \pm 5$ ps. This decay time, comparable to results in other experiments [42-45], reflects the non-radiative recombination of trions in the defect sites. The trion lifetime agrees with the THz recovery time under similar conditions ($\tau_2 = 29$ ps) [Fig. 2(c)].

To further verify the trion mechanism, we have conducted the THz experiment with tunable pump photon energy from 0.77 to 2.11 eV (Fig. 4). The overall THz dynamical response is

suppressed sharply and the major (long) component is quenched as the photon energy falls below 1.9 eV. This critical energy value matches the resonance of the A exciton and trion from the absorption spectrum of monolayer MoS_2 [Fig. 4(b)] [1,23]. Near the excitonic resonance, we expect only excitons and trions to be produced, with minimum free-carrier generation and carrier heating. As the neutral excitons don't interact with the THz radiation, the strong signal of negative photoconductivity must arise from the charged trions.

In the trion scheme, the reduction of conductivity is expected to saturate at a value proportional to the doping electron density, when most of the excess electrons are transformed into trions. To this end, we have examined the THz dynamics and PL of a MoS_2 sample at different doping stages. At the initial stage, the pristine sample exhibited pronounced THz response (black line in Fig. 5). Its PL spectrum was centered at the trion (A^-) recombination energy (1.844 eV), indicating strong unintentional electron doping [inset of Fig. 5(a)]. We next doped the sample with chemical solutions according to the method described in Ref. [46]. We first deposited F_4TCNQ molecules as *p*-type chemical dopants to lower the electron density of the sample [46]. The PL of the sample increased and the peak position blueshifted to the exciton energy (1.885 eV), indicating the suppression of trion formation [23,46]. Correspondingly, the THz response was suppressed and subsequently quenched. The response also saturated at lower pump fluence (red and green lines in Fig. 5). The process could be reversed by depositing NADH molecules as *n*-type dopants to increase the electron density [46]. Both the PL spectrum and the THz response were partially recovered (blue lines in Fig. 5). The observed doping dependence agrees qualitatively with the expected behavior for trion formation.

Finally, the trion formation provides a straightforward explanation for the ~70% reduction of THz conductivity in the saturation regime [Fig. 2(b)], which simply reflects the three-fold

increase of carrier effective mass. It also naturally accounts for the fluence and photon-energy dependence of the THz recovery time. As shown in the insets of Fig. 2(a) and 4(a), the long-component lifetime (τ_2) increases with increasing pump fluence or photon energy, both corresponding to the increase of trion density. Excitons and trions in MoS_2 decay predominantly through defect-mediated processes. The probability to trap a trion will decrease when the defect sites gradually fill up at increasing excitation density. This will prolong the trion lifetime and hence, the THz recovery time.

The evidence and analysis above strongly suggest that trion formation is the dominant mechanism for the negative photoconductivity in monolayer MoS_2, particularly the major (long) component of the THz dynamics. For THz response in a shorter time scale (~1 ps) and optical excitation below the photon energy of 1.8 eV, trion-trion annihilation, defect-mediated absorption and carrier heating effect might become important. These secondary factors are discussed in the Supplemental Material [30].

In conclusion, we have observed a dramatic reduction of THz conductivity in monolayer MoS_2 under optical excitation. This unusual phenomenon originates from the strong many-body interactions in the material, which convert the 2D electron gas into a charged trion gas with the same charge density but much heavier effective mass. Similar photoconductivity phenomena are expected in other 2D materials with strong trionic effects. Our research reveals that charge transport in 2D TMD materials can be conducted by trions, which respond to the electric field as free charged particles [41]. The trionic effects provide an important ingredient for the design and optimization of TMD-based optoelectronics. Although the influence of short-lived trions is small in devices with low mobility and long transport channels, their role is expected to become increasingly important as the sample quality improves and the device scales decrease. Compared

to free electrons, trions allow us to control the motion of excitons and of the associated PL and (pseudo)spin through an applied electric field. This unique feature provides new device concepts for developing novel excitonic and spintronic devices that are operational at room temperature.

We thank K. F. Mak, T. F. Heinz, X. D. Xu, W. R. Lambrecht, and V. Bulović for helpful discussions, L. Yu and E. J. Sie for transport and optical characterization of the samples. This research was supported by Department of Energy Office of Basic Energy Sciences Grant No DE-SC0006423. Y.H.L and J.K. acknowledge support from the National Science Foundation under award number NSF DMR 0845358.

References

[1] K. F. Mak, C. Lee, J. Hone, J. Shan, and T. F. Heinz, Phys. Rev. Lett. **105**, 4, 136805 (2010).

[2] A. Splendiani, L. Sun, Y. Zhang, T. Li, J. Kim, C.-Y. Chim, G. Galli, and F. Wang, Nano Lett. **10**, 1271 (2010).

[3] B. Radisavljevic, A. Radenovic, J. Brivio, V. Giacometti, and A. Kis, Nat. Nanotech. **6**, 147 (2011).

[4] O. Lopez-Sanchez, D. Lembke, M. Kayci, A. Radenovic, and A. Kis, Nat. Nanotech. **8**, 497 (2013).

[5] K. F. Mak, K. L. He, J. Shan, and T. F. Heinz, Nat. Nanotech. **7**, 494 (2012).

[6] H. L. Zeng, J. F. Dai, W. Yao, D. Xiao, and X. D. Cui, Nat. Nanotech. **7**, 490 (2012).

[7] T. Cao *et al.*, Nat. Commun. **3**, 5, 887 (2012).

[8] X. Xu, W. Yao, D. Xiao, and T. F. Heinz, Nat. Phys. **10**, 343 (2014).

[9] T. Cheiwchanchamnangij and W. R. L. Lambrecht, Phys. Rev. B **85**, 205302 (2012).

[10] A. Ramasubramaniam, Phys. Rev. B **86**, 115409 (2012).

[11] H.-P. Komsa and A. V. Krasheninnikov, Phys. Rev. B **86**, 241201 (2012).

[12] T. C. Berkelbach, M. S. Hybertsen, and D. R. Reichman, Phys. Rev. B **88**, 045318 (2013).

[13] D. Y. Qiu, F. H. da Jornada, and S. G. Louie, Phys. Rev. Lett. **111**, 216805 (2013).

[14] K. He, N. Kumar, L. Zhao, Z. Wang, K. F. Mak, H. Zhao, and J. Shan, Phys. Rev. Lett. **113**, 026803 (2014).

[15] A. Chernikov, T. C. Berkelbach, H. M. Hill, A. Rigosi, Y. Li, O. B. Aslan, D. R. Reichman, M. S. Hybertsen, and T. F. Heinz, Phys. Rev. Lett. **113**, 076802 (2014).

[16] Z. Ye, T. Cao, K. O'Brien, H. Zhu, X. Yin, Y. Wang, S. G. Louie, and X. Zhang, Nature **advance online publication** (2014).

[17] B. Zhu, X. Chen, and X. Cui, arXiv:1403.5108 (2014).

[18] M. M. Ugeda *et al.*, Nat. Mater. **advance online publication** (2014).

[19] G. Wang, X. Marie, I. Gerber, T. Amand, D. Lagarde, L. Bouet, M. Vidal, A. Balocchi, and B. Urbaszek, arXiv:1404.0056 (2014).

[20] A. Singh, G. Moody, S. Wu, Y. Wu, N. J. Ghimire, J. Yan, D. G. Mandrus, X. Xu, and X. Li, Phys. Rev. Lett. **112**, 216804 (2014).

[21] A. R. Klots *et al.*, arXiv:1403.6455 (2014).

[22] E. J. Sie, Y.-H. Lee, A. J. Frenzel, J. Kong, and N. Gedik, arXiv:1312.2918 (2014).

[23] K. F. Mak, K. L. He, C. Lee, G. H. Lee, J. Hone, T. F. Heinz, and J. Shan, Nat. Mater. **12**, 207 (2013).

[24] J. S. Ross *et al.*, Nat. Commun. **4**, 6, 1474 (2013).

[25] A. M. Jones *et al.*, Nat. Nanotech. **8**, 634 (2013).

[26] R. Ulbricht, E. Hendry, J. Shan, T. F. Heinz, and M. Bonn, Rev. Mod. Phys. **83**, 543 (2011).

[27] M. C. Beard, G. M. Turner, and C. A. Schmuttenmaer, Phys. Rev. B **62**, 15764 (2000).

[28] A. L. Powell, C. C. Button, J. S. Roberts, P. I. Rockett, H. G. Grimmeiss, and H. Pettersson, Phys. Rev. Lett. **67**, 3010 (1991).

[29] A. S. Chaves and H. Chacham, App. Phys. Lett. **66**, 727 (1995).

[30] See Supplemental Material for detailed information of experiment and analysis.

[31] A. J. Frenzel, C. H. Lui, W. Fang, N. L. Nair, P. K. Herring, P. Jarillo-Herrero, J. Kong, and N. Gedik, App. Phys. Lett. **102** (2013).

[32] A. J. Frenzel, C. H. Lui, Y. C. Shin, J. Kong, and N. Gedik, Phys. Rev. Lett. **113**, 056602 (2014).

[33] Y.-H. Lee *et al.*, Adv. Mater. **24**, 2320 (2012).

[34] Y.-H. Lee *et al.*, Nano Lett. **13**, 1852 (2013).

[35] M. C. Nuss and J. Orenstein, in *Millimeter and Submillimeter Wave Spectroscopy of Solids*, edited by G. Grüner1998), pp. Chap. 2.

[36] G. Jnawali, Y. Rao, H. Yan, and T. F. Heinz, Nano Lett. **13**, 524 (2013).

[37] K. F. Mak, C. Lee, J. Hone, J. Shan, and T. F. Heinz, Phys. Rev. Lett. **105**, 136805 (2010).

[38] E. Fortin and F. Raga, Phys. Rev. B **11**, 905 (1975).

[39] A. Tanaka, N. J. Watkins, and Y. Gao, Phys. Rev. B **67**, 113315 (2003).

[40] M. M. Furchi, D. K. Polyushkin, A. Pospischil, and T. Mueller, arXiv:1406.5640 (2014).

[41] D. Sanvitto, F. Pulizzi, A. J. Shields, P. C. M. Christianen, S. N. Holmes, M. Y. Simmons, D. A. Ritchie, J. C. Maan, and M. Pepper, Science **294**, 837 (2001).

[42] T. Korn, S. Heydrich, M. Hirmer, J. Schmutzler, and C. Schuller, Appl. Phys. Lett. **99**, 102109 (2011).

[43] H. Shi, R. Yan, S. Bertolazzi, J. Brivio, B. Gao, A. Kis, D. Jena, H. G. Xing, and L. Huang, ACS Nano **7**, 1072 (2012).

[44] R. Wang, B. A. Ruzicka, N. Kumar, M. Z. Bellus, H.-Y. Chiu, and H. Zhao, Phys. Rev. B **86**, 045406 (2012).

[45] A. M. van der Zande *et al.*, Nature Mater. **12**, 554 (2013).

[46] S. Mouri, Y. Miyauchi, and K. Matsuda, Nano Lett. **13**, 5944 (2013).

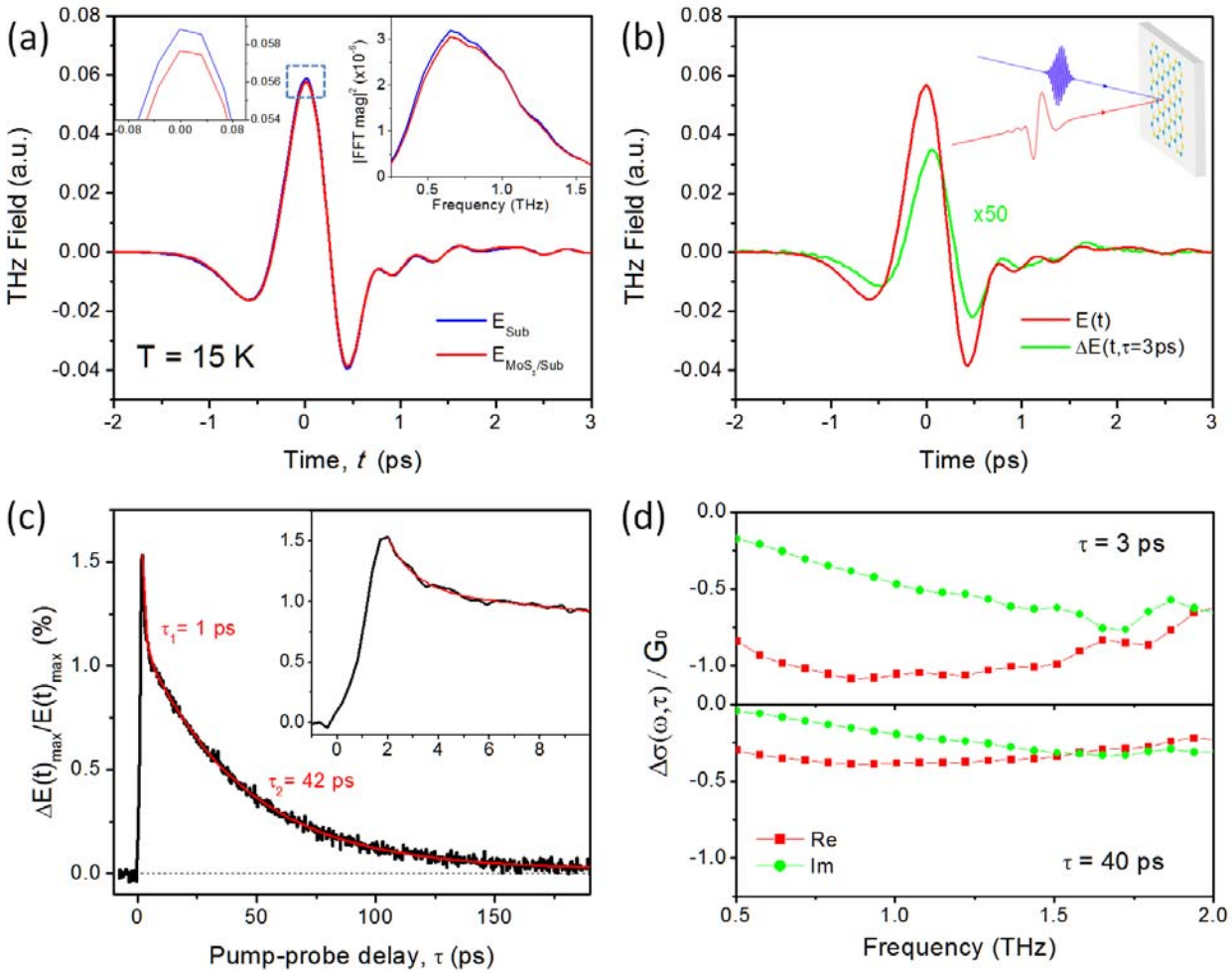

FIG. 1. (a) THz response of monolayer MoS_2 on a sapphire substrate in equilibrium conditions. The red and blue lines show the THz electric field transmitted through areas with and without the sample, respectively. The left inset is a zoomed-in view of the peak (dashed square). The measurement uncertainty at the peak is 3.5×10^{-5}, corresponding to 0.06% of the total THz signal. The right inset shows the THz power spectra. (b) Change of THz transmission after pulsed excitation. The red and green lines denote, respectively, the equilibrium transmitted THz field E(t) and the pump-induced waveform $\Delta E(t, \tau)$ at $\tau = 3$ ps. The inset is a schematic of our experiment. (c) Temporal evolution of the ratio between the maximum values of waveforms $\Delta E(t, \tau)$ and E(t). A biexponential fit (red line) yields lifetimes $\tau_1 = 1$ ps and $\tau_2 = 42$ ps. The inset

is a zoomed-in view of the short component. (d) The extracted pump-induced change of complex sheet conductivity $\Delta\sigma(\omega,\tau)$ at τ = 3 and 40 ps. The measurements were made at T = 15 K, with incident pump fluence 50 $\mu J/cm^2$ and photon energy 3.1 eV.

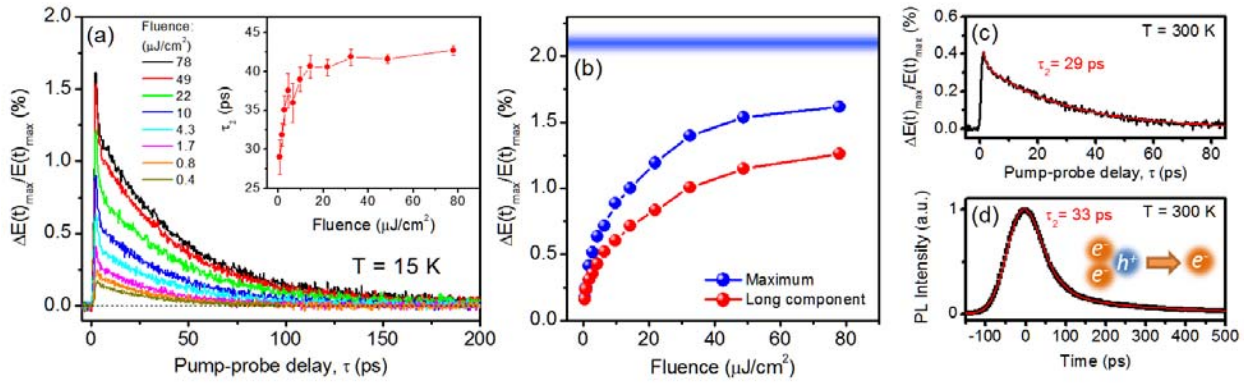

FIG. 2 (a) Temporal THz dynamics of monolayer MoS_2 at T = 15 K, as in Fig. 1(c), for different incident pump fluences, with excitation photon energy 3.1 eV. The inset shows the long-component lifetime (τ_2) from biexponential fits as a function of fluence. No systematic fluence dependence was found for the short-component lifetime ($\tau_1 \approx 1$ ps). (b) The maximum pump-induced signal (at $\tau \approx 2$ ps) and the long-component magnitude as a function of fluence. The blue bar at 2.1 ± 0.06 % denotes the total attenuation of THz field by the unexcited MoS_2 sample, as determined from Fig. 1(a). (c) THz dynamics at room temperature. A biexponential fit (red line) yields lifetimes $\tau_1 = 1.1$ ps and $\tau_2 = 29$ ps. (d) Time-resolved photoluminescence (PL) of monolayer MoS_2 at emission photon energies 1.7 - 2.0 eV. The red line is a biexponential fit, convolved with a Gaussian instrumental response function (standard deviation 36 ps). The best-fit lifetimes are $\tau_2 = 33 \pm 5$ ps and $\tau_3 = 230 \pm 10$ ps. The inset depicts trion recombination as the PL mechanism. In (c) and (d), we used pump fluence ~200 μJ/cm^2 and photon energy 3.1 eV.

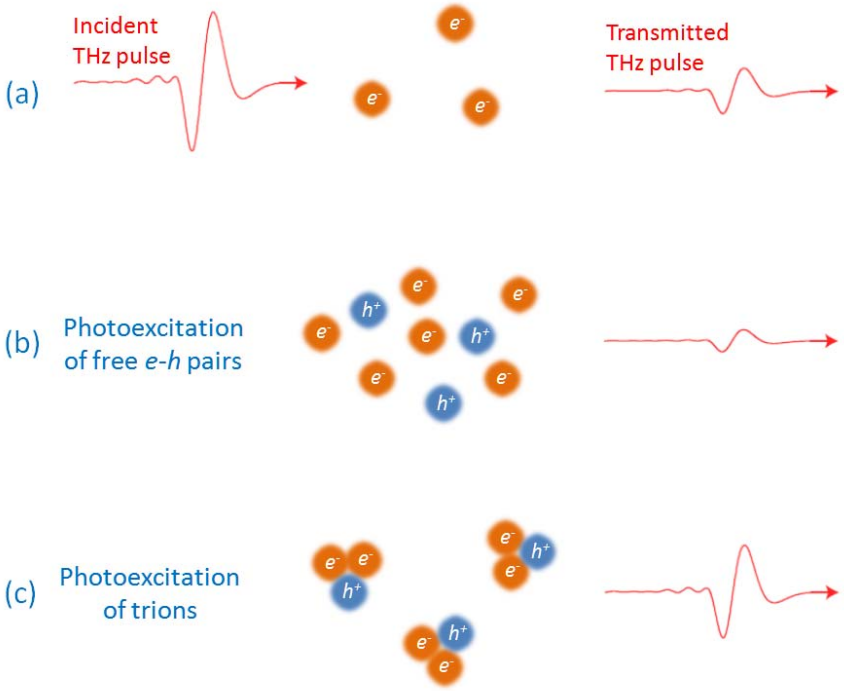

FIG. 3. Schematic of trionic effect on the THz response of a semiconductor under interband photoexcitation. (a) Absorption of THz pulse by doping-induced free carriers. (b) Increased THz absorption by excitation of free electron-hole pairs. (c) Reduced THz absorption by formation of trions.

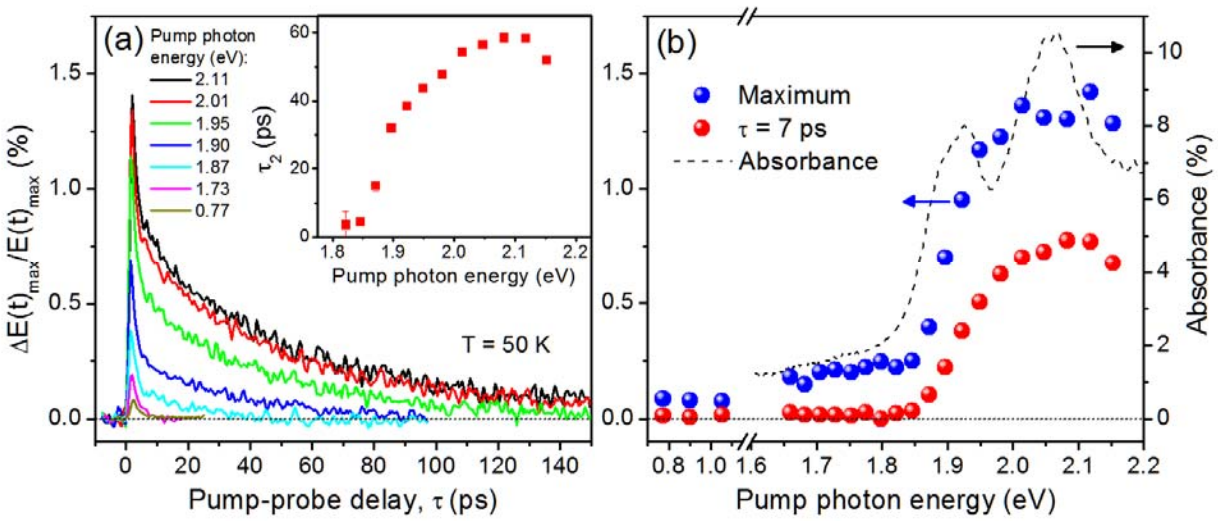

FIG. 4. (a) Temporal THz dynamics of monolayer MoS_2 at T = 50 K, with the same incident pump fluence (65 μJ/cm^2) but different pump photon energy (0.77 – 2.11 eV). The inset shows the long-component lifetime (τ_2) from biexponential fits as a function of photon energy. No systematic energy dependence was found for the short-component lifetime ($\tau_1 \approx 2$ ps). (b) The maximum pump-induced signal at $\tau \approx 2$ ps and at $\tau = 8$ ps (representing the long-component contribution) as a function of photon energy. The dashed curve is the absorption spectrum measured on a representative monolayer MoS_2 flake at T = 20 K using the method in Ref. [1].

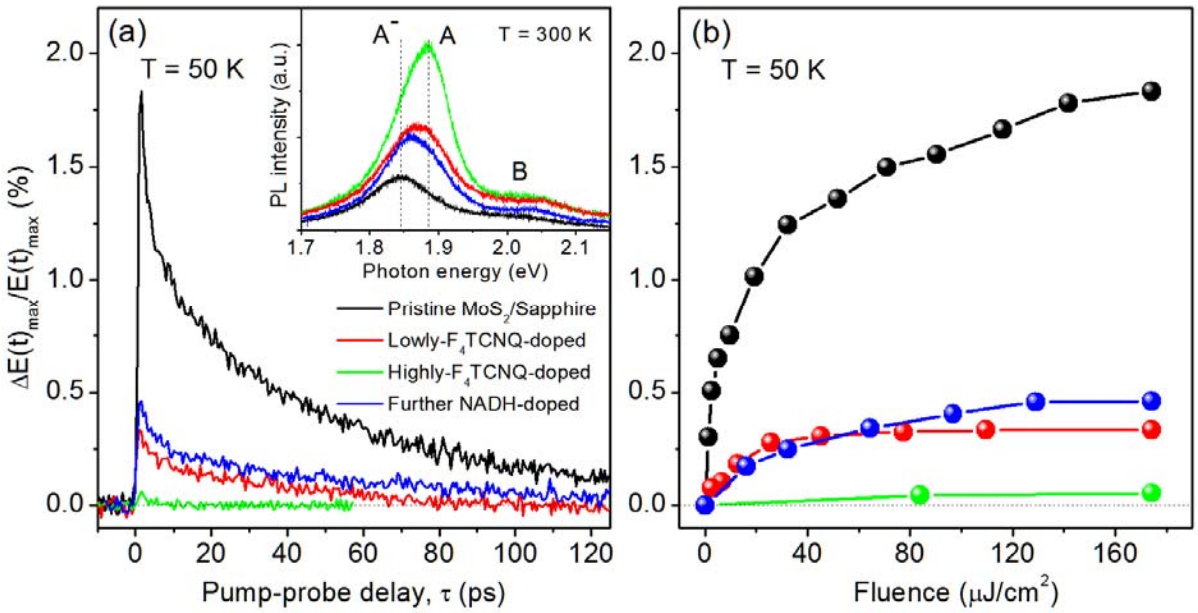

FIG. 5. (a) Temporal THz dynamics of monolayer MoS_2 at different chemical doping stages. The measurements were made on a pristine MoS_2 sample on sapphire (black), the same sample after being doped lightly (red) and heavily (green) with *p*-type F_4TCNQ molecules and further doped with *n*-type NADH molecules. The sample is different from that used in Fig. 2. All measurements were made with the same pump photon energy (1.98 eV) and fluence (174 $\mu J/cm^2$) at T = 50 K. The inset shows the PL spectra of the MoS_2 sample at the corresponding doping stages, taken at room temperature with 532-nm laser excitation. The A and B excitons and trion (A^-) are denoted. (b) The maximum pump-induced signal (at $\tau \approx 2$ ps) as a function of pump fluence at the corresponding doping stage at (a).